THE JOURNAL OF PHYSICAL CHEMISTRY C

Article

Cite This: J. Phys. Chem. C XXXX, XXX, XXX−XXX

pubs.acs.org/JPCC

Thickness-Dependent Reactivity of O_2 on Cu Layers Grown on Ru(0001) Surfaces

M. Ramos,[*,†] C. Díaz,[*,‡,§,∥] A. E. Martínez,[†] F. Martín,[‡,§,⊥] and H. F. Busnengo[†]

[†]Instituto de Física Rosario, CONICET and Universidad Nacional de Rosario, Bv. 27 de Febrero 210 bis, 2000 Rosario, Argentina

[‡]Departamento de Química, [§]Condensed Matter Physics Center (IFIMAC), and [∥]Institute for Advanced Research in Chemical Sciences (IAdChem), Universidad Autónoma de Madrid, 28049 Madrid, Spain

[⊥]Instituo Madrileño de Estudios Avanzados en Nanociencia (IMDEA-nanociencia), Cantoblanco, 28049 Madrid, Spain

ABSTRACT: The reaction of diatomic molecules on bimetallic surfaces, formed by one to few monolayers of a metal adsorbed on a different metal substrate, is relevant to understand the role of surface strain and substrate chemical binding in catalysis, which is interesting for industrial applications, challenges existing state-of-the-art theoretical methods, due to the additional complexity associated with having a molecule with triplet spin multiplicity. Here, we have studied the interaction of O_2 with $Cu_{xML}/Ru(0001)$ (x being the number of Cu monolayers), for which experimental data are available, by means of multidimensional classical dynamics simulations based on first-principles potential energy surfaces. Our results show, on the one hand, that the inclusion of the surface temperature on the simulations is essential to reproduce the experimental observations, and therefore, to analyze the physical mechanisms behind these observations, and, on the other hand, that electronic effects due to the binding between the two metallic species are only relevant for one Cu monolayer, whereas strain is responsible for the observed reactivity in O_2 interacting with $Cu_{(x\geq 2)ML}/Ru(0001)$.

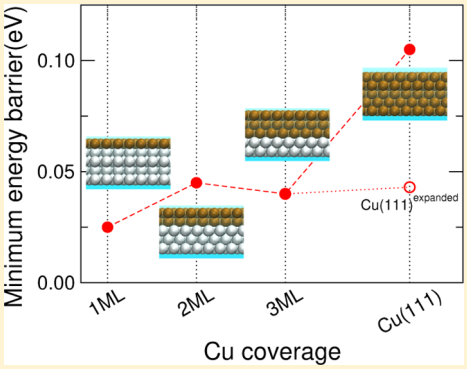

1. INTRODUCTION

Bimetallic surfaces, formed by a metal monolayer (ML) deposited on a metal substrate, exhibit electronic and chemical properties significantly different from those of the corresponding pristine metals.[1−9] When a ML of a metal is deposited on another metal surface, it often grows pseudomorphically adopting the lattice constant of the substrate, causing strain in the ML metal lattice. A second ML, on the other hand, may or not grows pseudomorphically. If it does not, the strain may give rise to periodic superstructures, whose average lattice constant is usually different from that of the individual metal lattices.[10] In some case, when the number of MLs further increases, the lattice constant of the top ML gets closer to the that of the parent bulk metal, thus decreasing the strain, until the lattice constant of the bulk metal is recovered and the strain disappears. This strain induces measurable changes on, for example, molecular reactivity[11,12] or vibrational frequencies of probe molecules.[13] However, the molecular reactivity observed on bimetallic systems not only depends on strain effects but also on the modifications in the electronic structure because of the binding of the surface atoms to the substrate atoms (hereafter called for short ligand effects).[1,2,14] For example, in ref 2, it was shown, by means of density functional theory (DFT) calculations, that the computed adsorption energies of CO on 1 and 2 ML of Pt pseudomorphically deposited on Ru(0001) were lower than the adsorption energy of CO on a compressed Pt(111)—a Pt(111) surface with a lattice parameter equal to that of Ru(0001).

Among bimetallic surfaces, Cu deposited on Ru(0001) has received a special attention.[15−25] For example, in 2000, Zajonz et al.[10] published a detailed analysis of the geometry of one and two MLs of Cu on Ru(0001), based on X-ray diffraction measurements. They observed that the first Cu ML grows pseudomorphically on Ru, leading to tensile strain on the surface, as the lattice constant in the Cu layer is 5.8% larger than in bulk Cu. In contrast, the second ML presents a stripe-phase reconstruction leading to a $16 \times \sqrt{3}$ superstructure, with an average lateral expansion of around 2.2%. More recently, Chakraborty et al.[26] have suggested, based on X-ray absorption spectroscopy measurements, that one or two ML thick Cu-patches on Ru are more active catalysts for ammonia oxidation than Ru, Cu, and three-dimensional (3D) Cu islands on Ru.

The interaction of diatomic molecules with Cu-covered Ru(0001) surfaces has been studied, for example, by Shimizu et al.,[27] using low-energy electron diffraction and thermal desorption spectroscopy. These authors have shown that H_2 sticking on Ru(0001) decreases drastically when Cu is deposited on the metal substrate. Similar results have been obtained later on by Laurent et al.[28,29] from multidimensional accurate simulations. More recently,[30] a combined experimental and theoretical analysis has shown an enhancement of

Received: May 7, 2018
Revised: June 11, 2018
Published: June 13, 2018

DOI: 10.1021/acs.jpcc.8b04354
J. Phys. Chem. C XXXX, XXX, XXX−XXX

H_2 diffraction probabilities on $Cu_{1ML}/Ru(0001)$ with respect to Cu(111) and Ru(0001), suggesting that both strain and ligand effects play a relevant role in $Cu_{1ML}/Ru(0001)$. Experiments have also been performed to determine sticking probabilities of O_2 as a function of the number Cu layers deposited on Ru. Otero et al.[31,32] have shown, using scanning tunneling microscopy (STM) techniques, that the O_2 sticking probability at thermal energies decreases by almost an order of magnitude when the Cu coverage increases from one to two MLs, and by almost two orders of magnitude from two to three MLs. Minniti et al.[33] have studied O_2 dissociative adsorption as a function of the incidence energy and the number of Cu MLs, using the King and Wells method[34] in a helium atom scattering apparatus.[35] They have found that two-Cu MLs' sticking curve is only shifted, toward higher energy, by about 40 meV with respect to the one-Cu ML curve. These authors argue that the high reactivity found for the case of two-Cu MLs cannot be understood only as a result of the tensile strain in the Cu ML, but also as a results of a strong influence of the substrate.

To get a deeper understanding of these experimental results, we have performed state-of-the-art dynamical simulations for $O_2/Cu(111)$, that can be seen as the limit case of infinite Cu overlayers, and $O_2/Cu_{xML}/Ru(0001)$ (x = 1 and 2). Simulations involving O_2 are a challenge for theory because of the singular nature of this molecule. The ground state of O_2 has a triplet spin multiplicity, which can change into singlet spin multiplicity when the molecule approaches the metal surface.[36−38] This means that the knowledge gained from theoretical studies involving diatomic molecules which singlet spin multiplicity, such as H_2,[39−41] N_2,[42−44] and CO,[7,45] cannot be straightforward extrapolated to O_2. For example, theoretical studies based on the Born−Oppenheimer static surface (BOSS) approximation do not even reproduce experimental trends for sticking in $O_2/Ag(100)$[38] or $O_2/Al(111)$.[37] The latter system is specially controversial because some authors[46,47] attribute this failure to an abrupt charge transfer from the metal-to-oxygen molecule, whereas others[37,48−50] attribute it to a triplet to singlet spin transition involving spin−orbit couplings. In our case, the spin−orbit coupling is stronger because the mass of Cu and Ru atoms are larger than that of Al. In the case of $O_2/Cu(111)$, very recent calculations based on the RPBE-DFT approach[51] reveal the activated character of the dissociation in agreement with experimental results.[33] This is in contrast with previous theoretical results based on the PW91-DFT approach,[11] which predicts nonactivated dissociation. Another issue to be considered is the effect of the energy exchange between the molecule and the surface. This effect has already been shown to play a relevant role in H_2/surface interactions,[52] one would expect that, for a heavier molecule like O_2, it could play an even more important role.[53,54]

In this manuscript, we show that multidimensional classical dynamics simulations, carried out on a DFT-based potential energy surface (PES), reproduce reasonably well the experimental results of ref 33, provided that energy dissipation into the substrate phonons is taken into account during the dynamics. Our simulations also allow us to understand the physical mechanisms responsible for these experimental observations.

2. THEORETICAL TOOLS

To carry out our dynamics study, we have worked within the Born−Oppenheimer approximation. Thus, we have first computed the continuous PES for $O_2/Cu_{xML}/Ru(0001)$ (x = 1,2) and $O_2/Cu(111)$. For this, we have applied the corrugation reducing procedure[55] to a set of DFT energy data. The required DFT energy data have been computed using the plane-wave based code VASP.[56−59] We have worked within the generalized gradient approximation framework using the semi-local RPBE exchange−correlation functional,[60] which was developed to improve the description of molecular adsorption of O_2, CO, and NO on metal surfaces provided, for instance, by the PBE[61] or PW91[62] functional.

To simulate the infinite nature of the surfaces, we have applied periodic boundary conditions in the x and y directions, whereas in the z direction, we have considered a five-layer slab, and a 12 Å vacuum region to avoid spurious interactions between neighboring slabs. The equilibrium surface geometries were obtained by allowing the three topmost layers to relax until the forces were lower than 0.02 eV/atom, while the two bottom layers were kept fixed at the calculated values of the corresponding metal in bulk phase, that is 2.12 Å for Cu(111) and 2.18 Å for Ru(0001) for the $Cu_{xML}/Ru(0001)$ with x = 1 and 2.

The interaction energies of O_2 with $Cu_{1ML}/Ru(0001)$ and Cu(111) have been computed using a (3×3) unit cell and a $(7 \times 7 \times 1)$ Monkhorst−Pack[63] grid of k-points. For $O_2/Cu_{2ML}/Ru(0001)$, a $(16 \times \sqrt{3})$ unit cell and a $(1 \times 7 \times 1)$ Monkhorst−Pack grid of k-points has been used to properly describe the experimentally observed reconstruction (see section 3.3 for further details). The energy cut-off for the plane wave expansion has been set to 450 eV and an electronic smearing has been introduced according to the Methfessel and Paxton scheme[64] with N = 1 and σ = 0.01 eV in all cases.

To perform dynamics simulations accounting for surface temperature effects, molecule-surface energy exchange, and energy dissipation to the bulk, we have used the generalized Langevin oscillators (GLO)[65,66] model as previously implemented by Busnengo et al.[67] (see Figure 1 for a schematic representation). In this approximation, to account for the molecule-surface energy exchange, the surface is allowed to oscillate as a 3D rigid oscillator of mass m_s and coordinates $\boldsymbol{R}_s = (X_s, Y_s, Z_s)$, m_s being the mass of a surface atom in the topmost layer. To introduce thermal fluctuations and energy dissipation to the bulk, a virtual 3D oscillator of mass m_v and coordinates $\boldsymbol{U}_s = (U_x, U_y, U_z)$, m_v being the mass of a bulk atom (bottom layer), is coupled to the surface oscillator. The coupling matrix between these oscillators includes a random force term and a damping term to simulate each of the

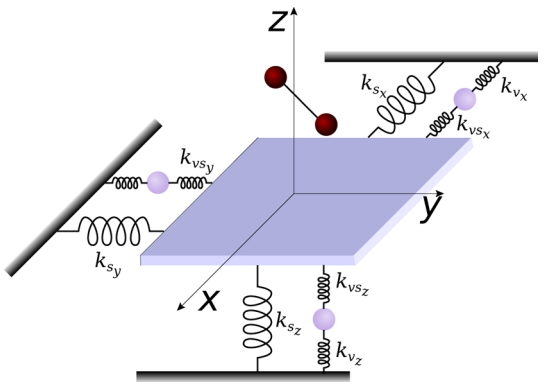

Figure 1. Schematic representation of the GLO model.

DOI: 10.1021/acs.jpcc.8b04354
J. Phys. Chem. C XXXX, XXX, XXX−XXX

aforementioned effects. Thus, applying the GLO method, the equations of motions are given by

$$m_{1,2}\frac{d^2\boldsymbol{R}_{1,2}}{dt^2} = -\nabla_{\boldsymbol{R}_{1,2}} V^{6D}(\boldsymbol{R}_1 - \boldsymbol{R}_s, \boldsymbol{R}_2 - \boldsymbol{R}_s) \quad (1)$$

$$m_s\frac{d^2\boldsymbol{R}_s}{dt^2} = -\nabla_{\boldsymbol{R}_s} V^{6D}(\boldsymbol{R}_1 - \boldsymbol{R}_s, \boldsymbol{R}_2 - \boldsymbol{R}_s) - (\hat{K}_s + \hat{K}_{vs})\boldsymbol{R}_s + \hat{K}_{vs}\boldsymbol{U}_s \quad (2)$$

$$m_v\frac{d^2\boldsymbol{U}_s}{dt^2} = -(\hat{K}_v + \hat{K}_{vs})\boldsymbol{U}_s + \hat{K}_{vs}\boldsymbol{R}_s - \hat{\gamma}_v\frac{d\boldsymbol{U}_s}{dt} + W(\Delta t) \quad (3)$$

where $\boldsymbol{R}_{1,2} = (X_{1,2}, Y_{1,2}, Z_{1,2})$ and $m_{1,2}$ represent the coordinates and masses of the oxygen atoms, respectively. $\hat{K}_s$ is the elastic coupling of the surface oscillator to the (fixed) bulk, $\hat{K}_v$ is the coupling of the virtual oscillator, and $\hat{K}_{vs}$ is the elastic coupling among both oscillators. The virtual oscillator is affected by a damping force characterized by the $\gamma\hat{K}_v$ matrix and a random force represented by $\boldsymbol{W}(\Delta t)$. The equations of motion (1−3) were integrated using the third order, fixed-step Beeman method.[68] In our set up, we considered the oscillators in the x and y directions as isotropic, that is, with identical elastic constants. The values of the parameters used were obtained by allowing one surface and/or one subsurface atom to oscillate in a given direction (x, y or z), fitting a harmonic potential and calculating the elastic coupling constant as $\frac{\partial^2 V}{\partial R_i^2}$ with $i = x, y, z$; the calculated values are given in Table 1.

Table 1. Elastic Coupling Constants for Each Oscillator in the GLO Model[a]

	$K_{s_{x,y}}$	K_{s_z}	$K_{v_{x,y}}$	K_{s_z}	$K_{vs_{x,y}}$	K_{vs_z}
Cu(111)	2.82	2.83	4.36	5.02	1.75	1.03
Cu_{1ML}/Ru(0001)	2.67	3.64	11.8	11.6	0.67	1.15

[a]All values are in 10^{-2} eV/Å^2.

3. RESULTS AND DISCUSSION

3.1. O_2/Cu(111). As already discussed in ref 51., a simple scrutiny of our computed RPBE-PES already reveals that the system is activated—in contrast with previous results based on PW91-DFT calculations[11]—with a minimum entrance barrier of 0.097 eV. This minimum barrier is found for the bridge-90-0 configuration (see Figure 2a), in which the molecule lies parallel to the surface, with its center of mass (CoM) over the bridge site and the two O atoms pointing to top sites. However, the high exit barrier (>1 eV) found for this configuration will prevent molecular dissociation. When the CoM of the molecule moves from the bridge site to the site located halfway between bridge and the opposite top site (see Figure 2c), the entrance barrier increases to 0.202 eV, but the exit barrier disappears. Thus, to dissociate, the O_2 molecule should approach the surface parallel to it over the bridge site, and later on it has to move quasi-parallel to the surface from the bridge to the hollow site—the reactive path is shown in Figure 2d. Interestingly, as can be observed in Figure 2, once the molecule overcomes the entrance-channel barrier, it encounters a molecular chemisorption well varying from −0.168 eV at the bridge-90-0 configuration (Figure 2a) to −0.284 eV at the bridge-to-bridge configuration (Figure 2c). The presence of these molecular wells plays a prominent role in this system as we discuss below. Here, it is important to point out that these are not chemisorption wells, but rather saddle points. The global chemisorption minimum in full 6D is found at the face-centered cubic (fcc)-90-30 configuration, with a depth of −0.317 eV.

To further scrutinize the characteristics of this system, we have carried out classical dynamics simulations. First, we consider normal incidence within the BOSS framework, that is, no energy exchange between the molecule and the surface is allowed. In Figure 3a, we display the dissociative adsorption probability, P_{ads}, as a function of the incidence normal energy ($E_\perp$). We observe a threshold at 0.09 eV, which is compatible with having an activated system. From this energy threshold, the probability increases with $E_\perp$ until it reaches a maximum of 0.38 at 0.2 eV. From this maximum, the probability decreases monotonically with the energy. To understand this behavior, we have performed a more detailed analysis of our classical trajectories. From the 2D-PES cuts shown in Figure 2, we can see the presence of reaction barriers in the entrance channel, $Z \approx 2.5$ Å. Thus, the molecule has to overcome this barrier to dissociate. From the analysis of the classical trajectories, we have found that the number of molecules reaching $Z < 2.5$ Å increases monotonically with $E_\perp$. In fact, for $E_\perp \geq 0.2$ eV, 100% of the molecules overcome the barrier. A molecule that actually dissociates can follow either a direct reaction path or an indirect one. In the latter case, hereafter called dynamic

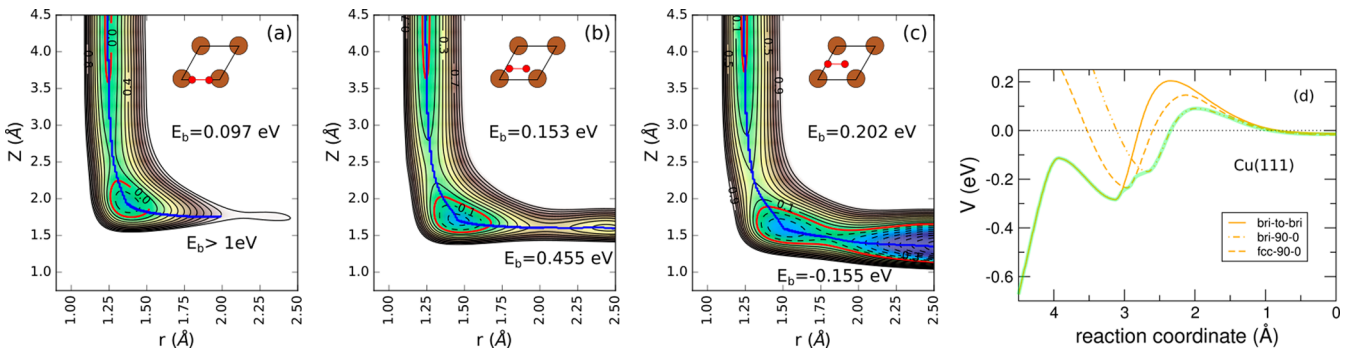

Figure 2. (a−c) 2D (r, Z_{CM}) for O_2/Cu(111) on bridge-90-0, fcc-90-0, and bridge-to-bridge configurations, respectively. The energy difference between consecutive equipotential lines is $\Delta E = 0.1$ eV; the red lines represent the 0 eV (reference energy level corresponding to the O_2 molecules and the surface in equilibrium and far from each other), whereas solid (dashed) lines correspond to positive (negative) potential energy values. The blue line indicates the minimum-energy path for that configuration. (d) Energy profile along the minimum-energy path for the three configurations.

DOI: 10.1021/acs.jpcc.8b04354
J. Phys. Chem. C XXXX, XXX, XXX−XXX

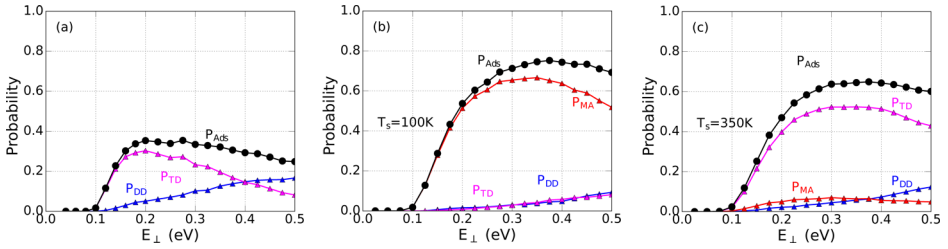

Figure 3. O_2 dissociation probability on Cu(111) as a function of the normal energy. Black circles: total dissociation probability; blue triangles: direct dissociation; magenta triangles: dissociation after trapping. (a) Static surface approximations; (b,c) GLO approximation with surface temperature 100 and 350 K, respectively. DD refers to direct dissociation, TD refers to dissociation after trapping, MA refers to molecular adsorption, and Ads refers to adsorption.

trapping, the molecule may rebound many times on the surface before finding a barrierless path and dissociate. To distinguish between these two mechanisms, we have chosen five as the number of rebounds that defines trapping. Figure 3a shows the calculated direct and the trapping dissociation probabilities according to this definition. One can see that direct dissociation increases monotonically with incidence energy, whereas the trapping dissociation shows the same non-monotonic behavior found for the total dissociation. For $E_\perp$ > 0.2 eV, the dissociation after trapping decreases when the energy increases because the molecules find more easily barrierless paths, whereas the number of molecules approaching the surface remains constant. The combination of direct and trapping dissociation explains the nonmonotonic behavior found for the dissociative adsorption of O_2 on Cu(111). However, the simulated dissociation probability agrees poorly with experimental sticking measurements.[33]

Digging deeper into the trapping mechanism, we have found that, at the lower energies, all molecules trapped on the surface end up dissociating because the same barriers that prevent the molecules from approaching directly the surface prevent them from escaping back to the vacuum after having overcome the barrier. At higher energies, on the one hand, some of the molecules trapped on the surface can escape to the vacuum (are reflected). We investigate now if this mechanism remains valid when we allow the molecule to exchange energy with the surface. For this, we have run classical dynamics simulations using the GLO method (see section 2). In Figure 3b,c, we show the GLO sticking probabilities obtained for a surface temperature T_s = 100 K and T_s = 350 K, respectively. In the same Figures, we also display the contribution of the different channels, namely, molecular adsorption, direct dissociation, and dissociation after trapping. The most interesting feature in these Figures is the presence of the molecular adsorption, which does not exist when the surface remains frozen. Remarkably, for the lower surface temperature (Figure 3b), the sticking probability is governed by molecular adsorption channel. In this case, after having overcome the barrier in the entrance channel, the molecule transfers energy to the surface, so that it does not have enough energy to overcome the barrier located in the exit channel (see Figure 2). For higher T_s (Figure 3c), on the other hand, the surface may transfer energy to the molecule, so that trapped molecules may find a barrierless path toward dissociation more easily, that is, they may overcome the exit barriers toward dissociation more easily, which explains why at T_s = 350 K the sticking curve is dominated by dissociation after trapping, and that the trapping dissociation curve decreases more slowly than in the case of BOSS simulations (Figure 3a). Thus, our results indicate that the molecule-surface energy exchange plays a key role in understanding the reactivity of this system.

We note that in our simulations we assign trajectories to the molecular adsorption if at the end of the integration time (80 ps), they have not dissociated or have not been scattered. To ensure that these adsorbed molecules are, in fact, in a molecular adsorption state, we have performed a detailed analysis of their final states. In Figure 4, we display the *XY*, *Z*, and θ distribution of the molecules assigned to the molecular adsorption channel [(a), (b) and (d)], as well as, their final energy (c). We show results for an incidence energy of 0.2 eV, but similar results are found for other values. In this Figure, we observe that adsorbed molecules lie mostly parallel to the surface 70° < θ < 110° (Figure 4a), at a distance 1.5 Å < *Z* < 1.8 Å over the surface (Figure 4b), and with their CoM located around the hollow sites (Figure 4d). Furthermore, their final energy has been found to range between −0.3 and −0.22 eV (Figure 4c), in very good agreement with the calculated depth of the chemisorption well. All these characteristics are compatible with the molecular adsorption states described above (see Figure 2).

3.2. O_2/Cu_{1ML}/Ru(0001). We have carried out the same analysis for O_2 dissociation on a ML of Cu adsorbed on Ru(0001). It has been found experimentally[10,31] that the first ML of Cu grows pseudomorphically on Ru(0001), that is, the Cu ML is strained with respect to its equilibrium geometry in Cu(111). Thus, strain and ligand effects[11,14,69] could be expected. In Figure 5, we show the 2D cuts, representing the electronic interaction of O_2 with Cu_{1ML}Ru(0001), for the same configurations as in Figure 2. The main features of these 2D cuts are very similar to those of the O_2/Cu(111) PES (Figure 2). The minimum reaction barrier, located at the entrance channel, is 0.026 eV for the bridge-90-0 configuration. In this configuration we also observe a molecular chemisorption well and a barrier of 0.675 eV in the exit channel. As in the case of O_2/Cu(111), to dissociate, the molecule has to move parallel to the surface from the bridge-90-0 configuration to the bridge-to-bridge one, after having overcome the first barrier (see Figure 5c). The main differences between the O_2/Cu(111) and the O_2/Cu_{1ML}Ru(0001) PESs are the height of the entrance and exit barriers, and the depth of the chemisorption wells. The minimum barrier for Cu_{1ML}/Ru(0001) is 0.026 eV, one-third of the value found for Cu(111). On the other hand, the depth of the global chemisorption well, located in the fcc-90-0 configuration, is −0.707 eV, that is, more than twice larger than for O_2/Cu(111).

As a consequence, the dynamical behavior of the O_2/Cu(111) and O_2/Cu_{1ML}Ru(0001) systems is very similar within the BOSS approximation. As Figure 6a shows, for the

DOI: 10.1021/acs.jpcc.8b04354
J. Phys. Chem. C XXXX, XXX, XXX−XXX

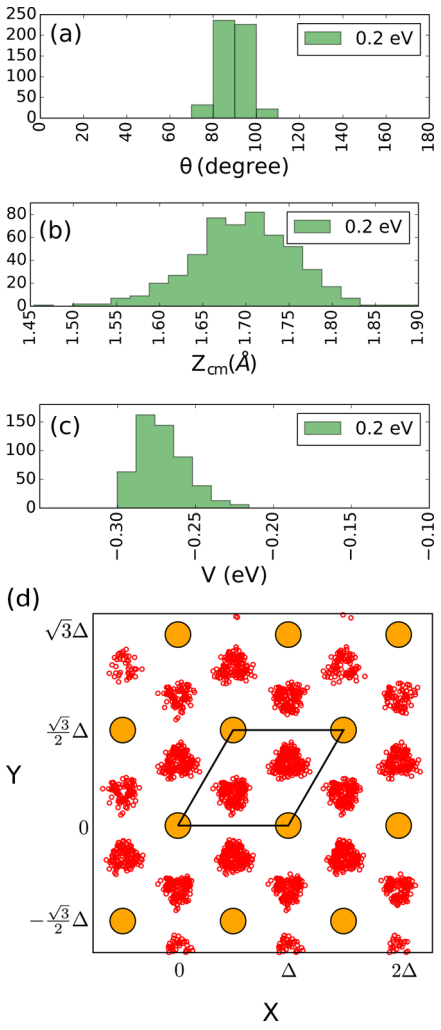

Figure 4. Final states of the trajectories labeled as molecular adsorption (a) θ_f-distribution; (b) Z_{cm}-distribution; (c) potential energy distribution; and (d) position of the CoM in the *xy*-plane (red circles) of O_2 molecules at the end of the simulation for all trajectories considered as molecular adsorption events. Brown circles represent Cu atoms in the uppermost atomic layer.

latter system, the dissociative adsorption probability exhibits a more pronounced nonmonotonic behavior, but the same two mechanisms contribute to it: direct dissociation, whose probability increases monotonically with the energy, and dynamic trapping, whose probability is responsible for the nonmonotonic behavior. If we allow the molecule to exchange energy with the surface (see Figure 6b,c), the total adsorption probability increases and its nonmonotonic behavior softens considerably, similarly to what we have found for Cu(111). However, the role of the different mechanisms that lead to molecular adsorption (sticking from the experimental point of view) is rather different from that found in the case of O_2 on Cu(111). For Cu_{1ML}/Ru(0001), molecular adsorption is only noticeable at T_s = 100 K, in clear contrast with results obtained for Cu(111), where molecular adsorption is also observed at 350 K. Furthermore, in the latter, surface molecular adsorption is by far the dominant mechanism at T_s = 100 K, which is not the case for the Cu_{1ML}/Ru(0001). These differences are the consequence of the different depths of the corresponding chemisorption wells and the different barriers heights.

For the sake of completeness, Figure 7 shows an analysis of the events labeled as molecular chemisorption. From Figure 7a, we can see that chemisorbed molecules lie mostly parallel to the surface ($70° \leq \theta \leq 110°$) at a *Z* distance between 1.50 and 1.80 Å (Figure 7b). The final energy of these molecules, from −0.68 to −0.54 eV (Figure 7c), agrees with the depth of the calculated chemisorption well. Also in agreement with the location of the chemisorption well, we have found that the CoM of the molecule lies on the hollow sites (Figure 7d).

3.3. O_2/Cu_{2ML}/Ru(0001). We have also studied sticking probabilities of O_2 on two MLs of copper adsorbed on ruthenium, Cu_{2ML}/Ru(0001). Because of the complexity of this system, our analysis is based only on electronic structure results. According to Zajonz et al.[10] when two ML of Cu are deposited on Ru(0001), the surface undergoes a reconstruction, involving both Cu layers, which leads to a much larger $16 \times \sqrt{3}$ unit cell (see Figure 8). We can divide this unit cell in three different regions, the fcc region in which the Cu atoms are on fcc positions over the Ru surface, the hexagonal close-packed (hcp) region with the Cu atoms on hcp positions, and the dislocation regions that connect fcc and hcp regions (see Figure 9). From Figure 9, we can see that the Cu−Cu nearest-neighbor distance in the hcp region is close to that in Cu(111), whereas in the fcc region the Cu−Cu distance is closer to the Ru−Ru one. This complex unit cell makes the task of computing a whole continuous PES unaffordable because of the large size of the unit cell that should be used to appropriately describe the interaction of the O_2 with the

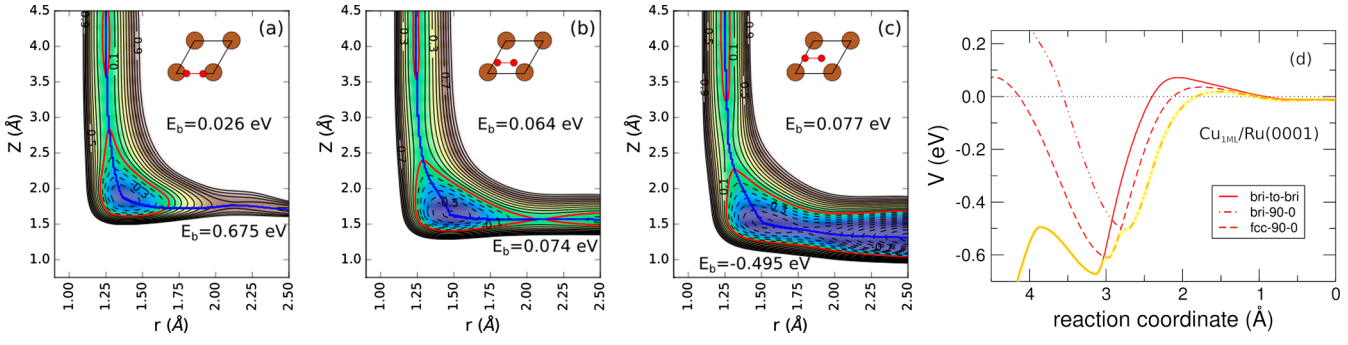

Figure 5. (a−c) 2D (r, Z_{CM}) for O_2/Cu_{1ML}/Ru(0001) on bridge-90-0, fcc-90-0, and bridge-to-bridge configurations, respectively. The energy difference between consecutive equipotential lines is ΔE = 0.1 eV; the red lines represent the 0 eV (reference energy level corresponding to O_2 and the surface in equilibrium and far from each other), whereas solid (dashed) lines correspond to positive (negative) potential energy values. The blue line indicates the minimum-energy path for that configuration. (d) Energy profile along the minimum-energy path for the three configurations.

DOI: 10.1021/acs.jpcc.8b04354
J. Phys. Chem. C XXXX, XXX, XXX−XXX

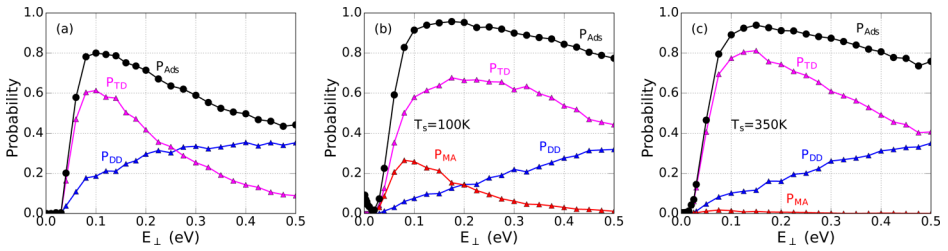

Figure 6. O_2 dissociation probability on $Cu_{1ML}Ru(0001)$ as a function of the normal energy. Black circles: total dissociation probability; blue triangles: direct dissociation; magenta triangles: dissociation after trapping. (a) SSA; (b) and (c) GLO approximation with surface temperature 100 and 350 K, respectively. DD refers to direct dissociation, TD refers to dissociation after trapping, MA refers to molecular adsorption, and Ads refers to adsorption.

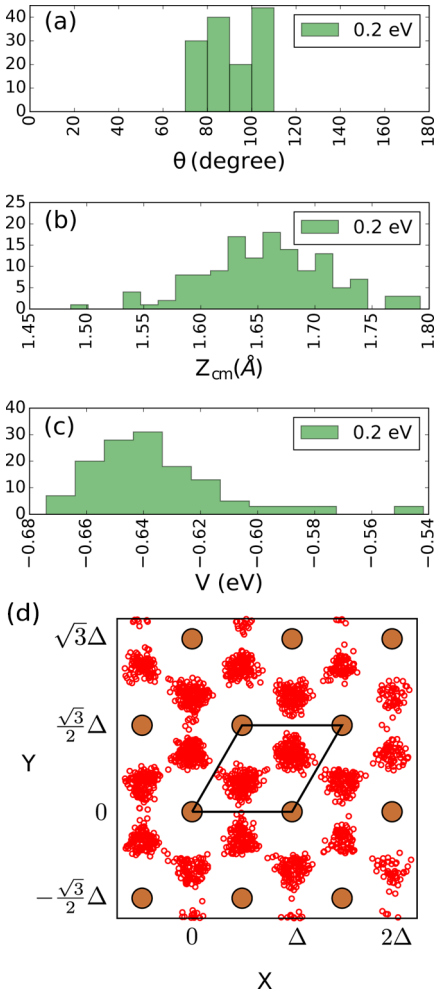

Figure 7. Final states of the trajectories labeled as molecular adsorption (a) potential energy distribution; (b) θ_f-distribution; (c) Z_{cm}-distribution; and (d) position of the CoM in the *xy*-plane (red circles) of O_2 molecules at the end of the simulation for all trajectories considered as molecular adsorption events. Brown circles represent Cu atoms in the uppermost atomic layer.

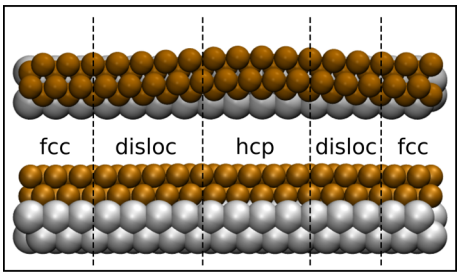

Figure 8. Upper and side views of the $16 \times \sqrt{3}$ unit cell used for $Cu_{2ML}/Ru(0001)$ slab. Brown (silver) balls represent Cu (Ru) atoms.

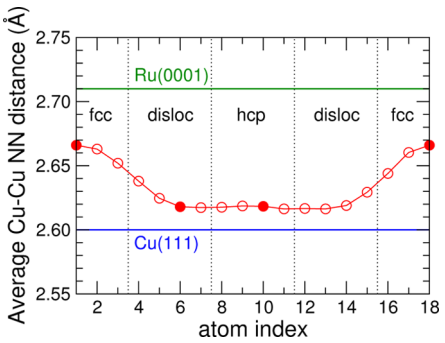

Figure 9. Average nearest-neighbor distance for each Cu atom located in the first atomic layer. Green (blue) line indicates the NN distance in Ru(0001) [Cu(111)] surface.

substrate. For this reason, we have only computed 2D cuts in the regions of the configuration space where the minimum energy barriers are expected to be located—we have assumed that the minimum reaction barriers will be located in the same regions as those in the $O_2/Cu_{1ML}Ru(0001)$ system.

In Figure 10a–c, we show the 2D cuts corresponding to the fcc region. The shape of these cuts are very similar to the ones obtained for $Cu_{1ML}/Ru(0001)$. The minimum barrier is only slightly higher than the one computed for $Cu_{1ML}/Ru(0001)$. As for Cu(111) and $Cu_{1ML}/Ru(0001)$, once the molecule has overcome the minimum reaction barrier, a parallel displacement of the molecule toward the hollow site is required to allow for dissociation. The 2D cuts computed for the hcp and dislocation regions are qualitatively similar to those computed for the fcc region. A detailed analysis of the 2D cuts containing the minimum reaction barriers in the three different regions reveals a substantial increase of the barrier heights, from 0.030 eV in the fcc region to 0.070 eV in the hcp and dislocation regions (see Figure 10d). Thus, the average minimum barrier along the unit cell is estimated to be of the order of 0.05 eV.

From these results, we can make an estimation of the adsorption probabilities by simply shifting the $O_2/Cu_{1ML}/Ru(0001)$ adsorption curve by an amount equal to the difference between the minimum reaction barrier in $O_2/Cu_{1ML}/Ru(0001)$ and the average minimum reaction barrier in $O_2/Cu_{2ML}/Ru(0001)$ (see Figure 11).

3.4. Comparison with Experiment. The validity of our theoretical approach and the subsequent analysis is supported

DOI: 10.1021/acs.jpcc.8b04354
J. Phys. Chem. C XXXX, XXX, XXX−XXX

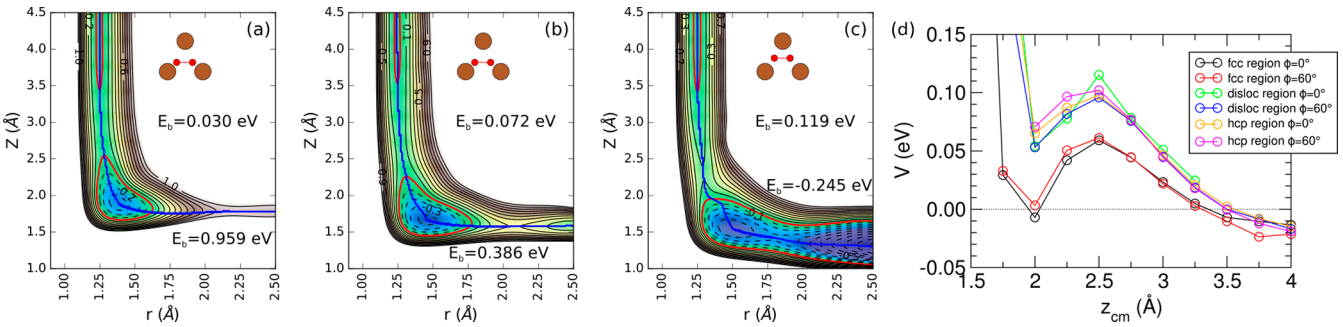

Figure 10. (a–c) p2D (r, Z_{CM}) for $O_2/Cu_{2ML}/Ru(0001)$ on bridge-90-0, fcc-90-0, and bridge-to-bridge configurations, respectively. The energy difference between consecutive equipotential lines is $\Delta E = 0.1$ eV; the red lines represent the 0 eV (reference energy level corresponding to O_2 and the surface in equilibrium and far from each other), whereas solid (dashed) lines correspond to positive (negative) potential energy values. The blue line indicates the minimum-energy path for that configuration. (d) Energy barrier in the entrance channel for the O_2 molecule approaching the surface in the different regions of the unit cell when the molecule is in its equilibrium distance and the internuclear vector is parallel to the surface.

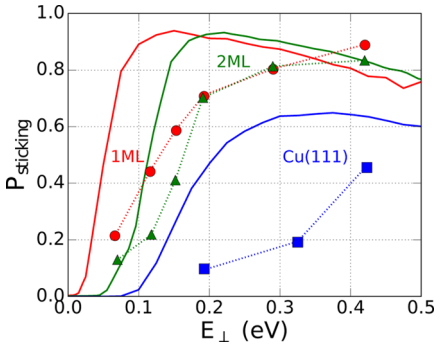

Figure 11. Sticking probability as a function of the perpendicular incidence energy. Solid line: theoretical simulations; symbols: experimental results from ref 33. (dotted lines are to guide the eyes).

by comparison with available experimental data for the three systems investigated in this work. In Figure 11, we compare the measured sticking probabilities[33] with our theoretical results. In qualitative agreement with experiment, our simulations for $O_2Cu_{1ML}/Ru(0001)$ and $O_2Cu_{2ML}/Ru(0001)$ show that at low incidence energies ($E_\perp$ < 0.2 eV) the sticking probability curves increase steeply, the latter being shifted toward higher incidence energies with respect to the former. At high incidence energies ($E_\perp \geq 0.2$ eV) both systems exhibit similar sticking probabilities, which barely change with $E_\perp$. The qualitative agreement with experiment further supports our theoretical analysis according to which molecular dissociation and molecular adsorption coexist and are both responsible for the sticking probability at low surface temperature. In the case of $O_2/Cu(111)$, an increasing behavior of the sticking probability is observed, in agreement with the experimental results. The co-existence of atomic and molecular oxygen, has been previously observed in experiments performed on other metal surfaces, such as Ag(110),[70−75] Pt(111),[72,76−78] Pd(111),[79−81] Cu(111),[82,83] and Cu(110).[84] Our simulations also agree with sticking probabilities inferred from STM techniques,[31] which show a swift decrease of the sticking probability with the number of Cu MLs at thermal energies. In this case, a direct comparison between our simulations and those STM measurements would require the knowledge of the Boltzmann distributions associated with these specific experiments, which are not available in the literature.

Finally, aiming at disentangling the role of ligand and strain effects in the reactivity of O_2 on $Cu_{xML}/Ru(0001)$, we have compared the minimum reaction barrier for 1, 2, and 3 Cu MLs adsorbed on Ru(0001) with the one for Cu(111), and with the reaction barrier obtained for a fictitious Cu(111) with a lattice parameter equal to the Ru lattice, that is, an expanded Cu(111). We note that the minimum barrier for 2ML and 3ML has been obtained by assuming pseudomorphic growth. From Figure 12, we can see that the barriers for 2ML, 3ML,

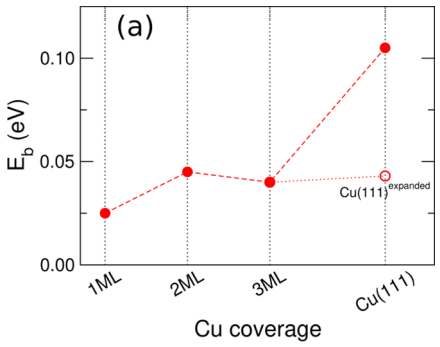

Figure 12. Minimum reaction barrier as a function of Cu MLs.

and the extended Cu(111) are very similar, higher than the barrier for 1ML and noticeable smaller than the barrier for Cu(111). This result suggests that the change of reactivity found experimentally is purely due to a strain effect for a number of MLs ≥ 2, whereas in the case of 1ML, both strain and ligand effects play a relevant role.

4. CONCLUSIONS

We have computed six-dimensional PESs for $O_2/Cu(111)$ and $O_2/Cu_{1ML}/Ru(0001)$ showing that these systems are activated, contrary to previous calculations but in agreement with experimental measurements. Our analysis of these PESs shows that the minimum-energy reaction path is rather complex. To dissociate, the molecule has to approach parallel, or almost parallel, to a bridge site of the surface, and subsequently it has to move from the bridge to a hollow site. Classical dynamics simulations using these PESs show that inclusion of energy exchange between the molecule and the surface is essential to qualitatively reproduce the behavior of the sticking probability found experimentally, and therefore to analyze the physical mechanisms behind this behavior. Our analysis reveals that although both PESs present a chemisorption well, the role of this well in the dynamics is rather different. Although for $O_2/Cu(111)$ sticking due to the

DOI: 10.1021/acs.jpcc.8b04354
J. Phys. Chem. C XXXX, XXX, XXX−XXX

molecular adsorption channel plays a significant role and is dominant at low surface temperature, for $O_2/Cu_{1ML}Ru(0001)$ this channel plays a minor role and is only perceptible at low surface temperature and low incidence energy. For this latter system molecular dissociation (mostly dissociation after trapping) is the dominant mechanism of sticking. Finally, our analysis of the minimum reaction barrier as a function of the number of Cu MLs, in comparison with a fictitious Cu(111) with an expanded lattice parameter equal to the Ru(0001) lattice reveals that effects due to the binding of Cu to the Ru substrate are only relevant for $Cu_{1ML}/Ru(0001)$, whereas strain effects dominate for $Cu_{(x\geq 2)ML}/Ru(0001)$.

AUTHOR INFORMATION

Corresponding Authors

*E-mail: ramos@ifir-conicet.gov.ar (M.R.).
*E-mail: cristina.diaz@uam.es (C.D.).

ORCID

M. Ramos: 0000-0001-8654-9501
F. Martín: 0000-0002-7529-925X

Notes

The authors declare no competing financial interest.

ACKNOWLEDGMENTS

The work was supported by CONICET project PIP 272, the UNR project PID ING534, the ANPCyT project PICT 2750, the MINECO Projects FIS2016-77889-R, the "Severo Ochoa" Programme for Centres of Excellence in R&D (SEV-2016-0686), the "María de Maetzu" Programme for Units of Excellence in R&D (MDM-2014-0377), and the CAM project no. S2013/MIT-2850. C.D.í acknowledges the Ramón y Cajal program of the MINECO. We also acknowledge computer time provided by the CCT-Rosario Computational Center, member of the High Performance Computing National System (SNCAD, MinCyT-Argentina) and also from CCC-UAM.

REFERENCES

(1) Rodriguez, J. Physical and chemical properties of bimetallic surfaces. *Surf. Sci. Rep.* **1996**, *24*, 223−287.
(2) Schlapka, A.; Lischka, M.; Groß, A.; Käsberger, U.; Jokob, P. Surface Strain versus Substrate Interaction in Heteroepitaxial Metal Layers: Pt on Ru(0001). *Phys. Rev. Lett.* **2003**, *91*, 016101.
(3) Xu, Y.; Ruban, A. V.; Mavrikakis, M. Adsorption and Dissociation of O2on Pt−Co and Pt−Fe Alloys. *J. Am. Chem. Soc.* **2004**, *126*, 4717−4725.
(4) Hoster, H.; Richter, B.; Behm, R. J. Catalytic Influence of Pt Monolayer Islands on the Hydrogen Electrochemistry of Ru(0001) Studied by Ultrahigh Vacuum Scanning Tunneling Microscopy and Cyclic Voltammetry†. *J. Phys. Chem. B* **2004**, *108*, 14780−14788.
(5) Kibler, L. A.; El-Aziz, A. M.; Hoyer, R.; Kolb, D. M. Tuning Reaction Rates by Lateral Strain in a Palladium Monolayer. *Angew. Chem., Int. Ed.* **2005**, *44*, 2080−2084.
(6) Groß, A. Reactivity of Bimetallic Systems Studied from First Principles. *Top. Catal.* **2006**, *37*, 29−39.
(7) Chen, J. G.; Menning, C. A.; Zellner, M. B. Monolayer Bimetallic Surfaces: Experimental and Theoretical Studies of Trends in Electronic and Chemical Properties. *Surf. Sci. Rep.* **2008**, *63*, 201−254.
(8) Groß, A. Tailoring the Reactivity of Bimetallic Overlayer and Surface Alloy Systems. *J. Phys.: Condens. Matter* **2009**, *21*, 084205.
(9) Wei, Z.; Sun, J.; Li, Y.; Datye, A. K.; Wang, Y. Bimetallic Catalysts for Hydrogen Generation. *Chem. Soc. Rev.* **2012**, *41*, 7994−8008.
(10) Zajonz, H.; Baddorf, A. P.; Gibbs, D.; Zehner, D. M. Structure of Pseudomorphic and Reconstructed Thin Cu Films on Ru(0001). *Phys. Rev. B: Condens. Matter Mater. Phys.* **2000**, *62*, 10436−10444.
(11) Xu, Y.; Mavrikakis, M. Adsorption and dissociation of O2 on Cu(): thermochemistry, reaction barrier and the effect of strain. *Surf. Sci.* **2001**, *494*, 131−144.
(12) Gsell, M.; Jakob, P.; Menzel, D. Effect of Substrate Strain on Adsorption. *Science* **1998**, *280*, 717−720.
(13) Kampshoff, E.; Hahn, E.; Kern, K. Correlation Between Surface Stress and the Vibrational Shift of CO Chemisorbed on Cu Surfaces. *Phys. Rev. Lett.* **1994**, *73*, 704−707.
(14) Laurent, G.; Busnengo, H. F.; Riviére, P.; Martín, F. h2 Reactivity on Strained Pseudomorphic Monolayers of Cu and Pd on Ru(0001). *Phys. Rev. B: Condens. Matter Mater. Phys.* **2008**, *77*, 193408.
(15) Christmann, K.; Ertl, G.; Shimizu, H. Model studies on bimetallic Cu/Ru catalysts I. Cu on Ru(0001). *J. Catal.* **1980**, *61*, 397−411.
(16) Houston, J. E.; Peden, C. H. F.; Blair, D. S.; Goodman, D. W. Monolayer and Multilayer Growth of Cu on the Ru(0001) Surface. *Surf. Sci.* **1986**, *167*, 427−436.
(17) Park, C.; Bauer, E.; Poppa, H. A Re-examination of the Cu/Ru(0001) System. *Surf. Sci.* **1987**, *187*, 86−97.
(18) Pötschke, G. O.; Behm, R. J. Interface Structure and Misfit Dislocations in Thin Cu Films on Ru(0001). *Phys. Rev. B: Condens. Matter Mater. Phys.* **1991**, *44*, 1442−1445.
(19) Wolter, H.; Schmidt, M.; Wandelt, K. Surfactant Induced Layer-by-layer Growth of Cu on Ru(0001) as Revealed by Oscillatory Work Function Changes. *Surf. Sci.* **1993**, *298*, 173−186.
(20) Feibelman, P. J.; Houston, J. E.; Davis, H. L.; O'Neill, D. G. Relaxation of the Clean, Cu- and H-covered Ru(0001) Surface. *Surf. Sci.* **1994**, *302*, 81−92.
(21) Günther, C.; Vrijmoeth, J.; Hwang, R. Q.; Behm, R. J. Strain Relaxation in Hexagonally Close-Packed Metal-Metal Interfaces. *Phys. Rev. Lett.* **1995**, *74*, 754−757.
(22) Stevens, J. L.; Hwang, R. Q. Strain Stabilized Alloying of Immiscible Metals in Thin Films. *Phys. Rev. Lett.* **1995**, *74*, 2078−2081.
(23) Schmid, A. K.; Bartelt, N. C.; Hamilton, J. C.; Carter, C. B.; Hwang, R. Q. Brownian Motion of Dislocations in Thin Films. *Phys. Rev. Lett.* **1997**, *78*, 3507−3510.
(24) Meinel, K.; Wolter, H.; Ammer, C.; Neddermeyer, H. A Misfit-induced Relaxation Structure of Epitaxial Cu Films on Ru(0001) and Its Potential Use for Nanostructuring. *Surf. Sci.* **1998**, *402−404*, 299−303.
(25) Wolter, H.; Meinel, K.; Ammer, C.; Wandelt, K.; Neddermeyer, H. O-induced Modification of Growth of Thin Cu Films on Ru(0001). *Phys. Rev. B: Condens. Matter Mater. Phys.* **1997**, *56*, 15459−15470.
(26) Chakraborty, D.; Damsgaard, C. D.; Silva, H.; Conradsen, C.; Olsen, J. L.; Carvalho, H. W. P.; Mutz, B.; Bligaard, T.; Hoffmann, M. J.; Grunwaldt, J.-D.; et al. Bottom-Up Design of a Copper-Ruthenium Nanoparticulate Catalyst for Low-Temperature Ammonia Oxidation. *Angew. Chem., Int. Ed.* **2017**, *56*, 8711−8715.
(27) Shimizu, H.; Christmann, K.; Ertl, G. Model studies on bimetallic Cu/Ru catalysts II. Adsorption of hydrogen. *J. Catal.* **1980**, *61*, 412−429.
(28) Laurent, G.; Martín, F.; Busnengo, H. F. Theoretical Study of Hydrogen Dissociative Adsorption on Strained Pseudomorphic Monolayers of Cu and Pd Deposited onto a Ru(0001) Substrate. *Phys. Chem. Chem. Phys.* **2009**, *11*, 7303−7311.
(29) Laurent, G.; Díaz, C.; Busnengo, H. F.; Martín, F. Non-monotonic Dissociative Adsorption of Vibrationally Excited h2 on Metal Surfaces. *Phys. Rev. B: Condens. Matter Mater. Phys.* **2010**, *81*, 161404.
(30) Díaz, C.; Martín, F.; Kroes, G. J.; Minniti, M.; Farías, D.; Miranda, R. H2 Diffraction from a Strained Pseudomorphic Monolayer of Cu Deposited on Ru(0001). *J. Phys. Chem. C* **2012**, *116*, 13671−13678.

DOI: 10.1021/acs.jpcc.8b04354
J. Phys. Chem. C XXXX, XXX, XXX−XXX

(31) Otero, R.; Calleja, F.; García-Suárez, V. M.; Hinarejos, J. J.; de la Figuera, J.; Ferrer, J.; de Parga, A. L. V.; Miranda, R. Tailoring Surface Electronic States Via Strain to Control Adsorption: O/Cu/Ru(0001). *Surf. Sci.* **2004**, *550*, 65−72.
(32) Calleja, F.; García-Suárez, V. M.; Hinarejos, J. J.; Ferrer, J.; de Parga, A. L. V.; Miranda, R. Relationship Between Strain and the Surface Electronic Structure of Cu(111) Films on Ru(0001): Theory and Experiment. *Phys. Rev. B: Condens. Matter Mater. Phys.* **2005**, *71*, 125412.
(33) Minniti, M.; Farías, D.; Perna, P.; Miranda, R. Enhanced Selectivity Towards O2 and H2 Dissociation on Ultrathin Cu Films on Ru(0001). *J. Chem. Phys.* **2012**, *137*, 074706.
(34) King, D. A.; Wells, M. G. Reaction Mechanism in Chemisorption Kinetics: Nitrogen on the Plane of Tungsten. *Proc. R. Soc. London, Ser. A* **1974**, *339*, 245−269.
(35) Nieto, P.; Barredo, D.; Farías, D.; Miranda, R. In-Plane and Out-of-Plane Diffraction of H2from Ru(001). *J. Phys. Chem. A* **2011**, *115*, 7283−7290.
(36) Yourdshahyan, Y.; Razaznejad, B.; Lundqvist, B. I. Adiabatic Potential Energy Surface of O2/Al(111): Rare Entrance-channel Barriers but Molecularly Chemisorbed State Apt for Abstraction. *Solid State Commun.* **2001**, *117*, 531−535.
(37) Behler, J.; Delley, B.; Lorenz, S.; Reuter, K.; Scheffler, M. Dissociation of O2 at Al(111): The Role of Spin Selection Rules. *Phys. Rev. Lett.* **2005**, *94*, 036104.
(38) Alducin, M.; Busnengo, H. F.; Muiño, R. D. Dissociative Dynamics of Spin-triplet and Spin-singlet o2 on Ag(100). *J. Chem. Phys.* **2008**, *129*, 224702.
(39) Nieto, P.; Pijper, E.; Barredo, D.; Laurent, G.; Olsen, R. A.; Baerends, E.-J.; Kroes, G.-J.; Farías, D. Reactive and Nonreactive Scattering of H2 from a Metal Surface Is Electronically Adiabatic. *Science* **2006**, *312*, 86−89.
(40) Diaz, C.; Pijper, E.; Olsen, R. A.; Busnengo, H. F.; Auerbach, D. J.; Kroes, G. J. Chemically Accurate Simulation of a Prototypical Surface Reaction: H2 Dissociation on Cu(111). *Science* **2009**, *326*, 832−834.
(41) Kroes, G.-J.; Díaz, C. Quantum and Classical Dynamics of Reactive Scattering of H2 from Metal Surfaces. *Chem. Soc. Rev.* **2016**, *45*, 3658−3700.
(42) Díaz, C.; Vincent, J. K.; Krishnamohan, G. P.; Olsen, R. A.; Kroes, G. J.; Honkala, K.; Nørskov, J. K. Multidimensional Effects on Dissociation of n2 on Ru(0001). *Phys. Rev. Lett.* **2006**, *96*, 096102.
(43) Alducin, M.; Muiño, R. D.; Juaristi, J. I. In *Dynamics of Gas-Surface Interactions: Atomic-Level Understanding of Scattering Processes at Surfaces*; Díez Muiño, R., Busnengo, H. F., Eds.; Springer Berlin Heidelberg: Berlin, Heidelberg, 2013; pp 371−388.
(44) Goikoetxea, I.; Juaristi, J. I.; Muiño, R.; Alducin, M. Surface Strain Improves Molecular Adsorption but Hampers Dissociation for on the Surface. *Phys. Rev. Lett.* **2014**, *113*, 066103.
(45) Hammer, B.; Morikawa, Y.; Nørskov, J. K. CO Chemisorption at Metal Surfaces and Overlayers. *Phys. Rev. Lett.* **1996**, *76*, 2141−2144.
(46) Libisch, F.; Huang, C.; Liao, P.; Pavone, M.; Carter, E. A. Origin of the Energy Barrier to Chemical Reactions of O2 on Al(111): Evidence for Charge Transfer, Not Spin Selection. *Phys. Rev. Lett.* **2012**, *109*, 198303.
(47) Cheng, J.; Libisch, F.; Carter, E. A. Dissociative Adsorption of O2 on Al(111): The Role of Orientational Degrees of Freedom. *J. Phys. Chem. Lett.* **2015**, *6*, 1661−1665.
(48) Behler, J.; Delley, B.; Reuter, K.; Scheffler, M. Nonadiabatic Potential Energy Surfaces by Constrained Density Functional Theory. *Phys. Rev. B: Condens. Matter Mater. Phys.* **2007**, *75*, 115409.
(49) Carbogno, C.; Behler, J.; Groß, A.; Reuter, K. Fingerprints for Spin-Selection Rules in the Interaction Dynamics of at Al(111). *Phys. Rev. Lett.* **2008**, *101*, 096104.
(50) Carbogno, C.; Behler, J.; Reuter, K.; Groß, A. Signatures of Nonadiabatic Dissociation at Al(111): First-principles Fewest-switches Study. *Phys. Rev. B: Condens. Matter Mater. Phys.* **2010**, *81*, 035410.
(51) Ramos, M.; Díaz, C.; Martínez, A. E.; Busnengo, H. F.; Martín, F. Dissociative and non-dissociative adsorption of O2 on Cu(111) and CuML/Ru(0001) surfaces: adiabaticity takes over. *Phys. Chem. Chem. Phys.* **2017**, *19*, 10217−10221.
(52) Nattino, F.; Díaz, C.; Jackson, B.; Kroes, G.-J. Effect of Surface Motion on the Rotational Quadrupole Alignment Parameter of Reacting on Cu(111). *Phys. Rev. Lett.* **2012**, *108*, 236104.
(53) Groß, A.; Eichler, A.; Hafner, J.; Mehl, M. J.; Papaconstantopoulos, D. A. Ab Initio Based Tight-binding Molecular Dynamics Simulation of the Sticking and Scattering of O2Pt(111). *J. Chem. Phys.* **2006**, *124*, 174713.
(54) Meyer, J.; Reuter, K. Modeling Heat Dissipation at the Nanoscale: An Embedding Approach for Chemical Reaction Dynamics on Metal Surfaces. *Angew. Chem., Int. Ed.* **2014**, *53*, 4721−4724.
(55) Busnengo, H. F.; Salin, A.; Dong, W. Representation of the 6D Potential Energy Surface for a Diatomic Molecule Near a Solid Surface. *J. Chem. Phys.* **2000**, *112*, 7641−7651.
(56) Kresse, G.; Hafner, J. Ab initio molecular dynamics for liquid metals. *Phys. Rev. B: Condens. Matter Mater. Phys.* **1993**, *47*, 558−561.
(57) Kresse, G.; Hafner, J. Ab initio molecular-dynamics simulation of the liquid-metal-amorphous-semiconductor transition in germanium. *Phys. Rev. B: Condens. Matter Mater. Phys.* **1994**, *49*, 14251−14269.
(58) Kresse, G.; Furthmüller, J. Efficiency of Ab-Initio Total Energy Calculations for Metals and Semiconductors Using a Plane-Wave Basis Set. *Comput. Mater. Sci.* **1996**, *6*, 15−50.
(59) Kresse, G.; Furthmüller, J. Efficient iterative schemes for ab initio total-energy calculations using a plane-wave basis set. *Phys. Rev. B: Condens. Matter Mater. Phys.* **1996**, *54*, 11169−11186.
(60) Hammer, B.; Hansen, L. B.; Nørskov, J. K. Improved adsorption energetics within density-functional theory using revised Perdew-Burke-Ernzerhof functionals. *Phys. Rev. B: Condens. Matter Mater. Phys.* **1999**, *59*, 7413−7421.
(61) Perdew, J. P.; Burke, K.; Ernzerhof, M. Generalized Gradient Approximation Made Simple. *Phys. Rev. Lett.* **1996**, *77*, 3865−3868.
(62) Perdew, J. P.; Chevary, J. A.; Vosko, S. H.; Jackson, K. A.; Pederson, M. R.; Singh, D. J.; Fiolhais, C. Atoms, Molecules, Solids, and Surfaces: Applications of the Generalized Gradient Approximation for Exchange and Correlation. *Phys. Rev. B: Condens. Matter Mater. Phys.* **1992**, *46*, 6671−6687.
(63) Monkhorst, H. J.; Pack, J. D. Special Points for Brillouin-Zone Integrations. *Phys. Rev. B: Condens. Matter Mater. Phys.* **1976**, *13*, 5188−5192.
(64) Methfessel, M.; Paxton, A. T. High-Precision Sampling for Brillouin-Zone Integration in Metals. *Phys. Rev. B: Condens. Matter Mater. Phys.* **1989**, *40*, 3616−3621.
(65) Adelman, S. A.; Doll, J. D. Generalized Langevin equation approach for atom/solid-surface scattering: General formulation for classical scattering off harmonic solids. *J. Chem. Phys.* **1976**, *64*, 2375.
(66) Tully, J. C.; Gilmer, G. H.; Shugard, M. Molecular Dynamics of Surface Diffusion. I. The Motion of Adatoms and Clusters. *J. Chem. Phys.* **1979**, *71*, 1630−1642.
(67) Busnengo, H. F.; Di Césare, M. A.; Dong, W.; Salin, A. Surface Temperature Effects in Dynamic Trapping Mediated Adsorption of Light Molecules on Metal Surfaces: H on Pd(111) and Pd(110). *Phys. Rev. B: Condens. Matter Mater. Phys.* **2005**, *72*, 125411.
(68) Beeman, D. Some Multistep Methods for Use in Molecular Dynamics Calculations. *J. Comput. Phys.* **1976**, *20*, 130−139.
(69) Sakong, S.; Groß, A. Dissociative Adsorption of Hydrogen on Strained Cu Surfaces. *Surf. Sci.* **2003**, *525*, 107−118.
(70) Sexton, B. A.; Madix, R. J. Vibrational Spectra of Molecular and Atomic Oxygen on Ag(11O). *Chem. Phys. Lett.* **1980**, *76*, 294−297.
(71) Prince, K. C.; Paolucci, G.; Bradshaw, A. M. Oxygen Adsorption on Silver (110): Dispersion, Bonding and Precursor State. *Surf. Sci.* **1986**, *175*, 101−122.
(72) Zhu, X.-Y.; Hatch, S. R.; Campion, A.; White, J. M. Surface Photochemistry. II. Wavelength Dependences of Photoinduced

DOI: 10.1021/acs.jpcc.8b04354
J. Phys. Chem. C XXXX, XXX, XXX−XXX

Dissociation, Desorption, and Rearrangement of O2 on Pt(111). *J. Chem. Phys.* **1989**, *91*, 5011−5020.
(73) Vattuone, L.; Rocca, M.; Restelli, P.; Pupo, M.; Boragno, C.; Valbusa, U. Low-temperature dissocation ofO2on Ag(110): Surface disorder and reconstruction. *Phys. Rev. B: Condens. Matter Mater. Phys.* **1994**, *49*, 5113−5116.
(74) Vattuone, L.; Rocca, M.; Valbusa, U. Anharmonic Shift in the Stretching Frequency of O2 Chemisorbed on Ag (110). *Surf. Sci.* **1994**, *314*, L904−L908.
(75) Pawela-Crew, J.; Madix, R. J.; Stöhr, J. The Effect of Subsurface Oxygen on the Orientation of Molecular Oxygen on Ag(110). *Surf. Sci.* **1995**, *339*, 23−28.
(76) Gland, J. L.; Sexton, B. A.; Fisher, G. B. Oxygen Interactions with the Pt(111) Surface. *Surf. Sci.* **1980**, *95*, 587−602.
(77) Avery, N. R. An EELS and TDS Study of Molecular Oxygen Desorption and Decomposition on Pt(111). *Chem. Phys. Lett.* **1983**, *96*, 371−373.
(78) Wurth, W.; Stöhr, J.; Feulner, P.; Pan, X.; Bauchspiess, K. R.; Baba, Y.; Hudel, E.; Rocker, G.; Menzel, D. Bonding, structure, and magnetism of physisorbed and chemisorbedO2on Pt(111). *Phys. Rev. Lett.* **1990**, *65*, 2426−2429.
(79) Imbihl, R.; Demuth, J. E. Adsorption of Oxygen on a Pd(111) Surface Studied by High Resolution Electron Energy Loss Spectroscopy (EELS). *Surf. Sci.* **1986**, *173*, 395−410.
(80) Hanley, L.; Guo, X.; Yates, J. T. Photolysis of Chemisorbed Dioxygen on Pd(111): Dependence on Photon Energy. *J. Chem. Phys.* **1989**, *91*, 7220−7227.
(81) Wolf, M.; Hasselbrink, E.; White, J. M.; Ertl, G. The Adsorbate State Specific Photochemistry of Dioxygen on Pd(111). *J. Chem. Phys.* **1990**, *93*, 5327−5336.
(82) Yokoyama, T.; Arvanitis, D.; Lederer, T.; Tischer, M.; Tröger, L.; Baberschke, K.; Comelli, G. Adsorption of oxygen on Cu(100). II. Molecular adsorption and dissociation by means of OK-edge x-ray-absorption fine structure. *Phys. Rev. B: Condens. Matter Mater. Phys.* **1993**, *48*, 15405−15416.
(83) Sueyoshi, T.; Sasaki, T.; Iwasawa, Y. Molecular and atomic adsorption states of oxygen on Cu(111) at 100-300 K. *Surf. Sci.* **1996**, *365*, 310−318.
(84) van Daelen, M. A.; Neurock, M.; van Santen, R. A. Reactivity of Diatomic Molecules on Cu(100). *Surf. Sci.* **1998**, *417*, 247−260.

DOI: 10.1021/acs.jpcc.8b04354
J. Phys. Chem. C XXXX, XXX, XXX−XXX